

# Low-energy structure of $^{61}\text{Mn}$ populated following $\beta$ decay of $^{61}\text{Cr}$

H.L. Crawford,<sup>1,2</sup> P.F. Mantica,<sup>1,2</sup> J.S. Berryman,<sup>1,2</sup> R. Broda,<sup>3</sup> B. Fornal,<sup>3</sup>  
 C.R. Hoffman,<sup>4</sup> N. Hoteling,<sup>5,6</sup> R.V.F. Janssens,<sup>5</sup> S.M. Lenzi,<sup>7,8</sup> J. Pereira,<sup>2,9</sup>  
 J.B. Stoker,<sup>1,2</sup> S.L. Tabor,<sup>4</sup> W.B. Walters,<sup>6</sup> X. Wang,<sup>5,10</sup> and S. Zhu<sup>5</sup>

<sup>1</sup> *Department of Chemistry, Michigan State University,  
 East Lansing, Michigan 48824, USA*

<sup>2</sup> *National Superconducting Cyclotron Laboratory,  
 Michigan State University, East Lansing, Michigan 48824, USA*

<sup>3</sup> *Institute of Nuclear Physics, Polish Academy of Sciences, Cracow PL-31342, Poland*

<sup>4</sup> *Department of Physics and Astronomy,  
 Florida State University, Tallahassee, FL 32306, USA*

<sup>5</sup> *Physics Division, Argonne National Laboratory, Argonne, Illinois 60429, USA*

<sup>6</sup> *Department of Chemistry and Biochemistry,  
 University of Maryland, College Park, MD 20742, USA*

<sup>7</sup> *Department of Physics, Padova University, I-35131 Padova, Italy*

<sup>8</sup> *National Institute of Nuclear Physics,  
 Padova Section, I-35131 Padova, Italy*

<sup>9</sup> *Joint Institute for Nuclear Astrophysics,  
 Michigan State University, East Lansing, MI 48824, USA and*

<sup>10</sup> *Department of Physics, University of Notre Dame, South Bend, IN 46556, USA*

(Dated: November 9, 2018)

## Abstract

$\beta$  decay of the  $^{61}\text{Cr}_{37}$  ground state has been studied. A new half-life of  $233 \pm 11$  ms has been deduced, and seven delayed  $\gamma$  rays have been assigned to the daughter,  $^{61}\text{Mn}_{36}$ . The low-energy level structure of  $^{61}\text{Mn}_{36}$  is similar to that of the less neutron-rich  $^{57,59}\text{Mn}$  nuclei. The odd- $A$   $^{25}\text{Mn}$  isotopes follow the systematic trend in the yrast states of the even-even,  $Z + 1$   $^{26}\text{Fe}$  isotopes, and not that of the  $Z - 1$   $^{24}\text{Cr}$  isotopes, where a possible onset of collectivity has been suggested to occur already at  $N = 36$ .

PACS numbers: 23.40.-s, 23.20.Lv, 21.60.Cs, 29.38.Db, 27.50.+e

## I. INTRODUCTION

According to the shell model, the  $1g_{9/2}$  single-particle orbital is well separated from the  $1g_{7/2}$ ,  $2d_{5/2}$  and other higher-energy orbitals, giving rise to the well-established  $N, Z = 50$  magic numbers. A less pronounced subshell closure for  $N, Z = 40$  is also expected, as a smaller energy gap typically occurs between the  $1g_{9/2}$  level and the lower  $pf$ -shell model states. However, collectivity is evident for most nuclei with  $N \sim Z \sim 40$ , and rotational-like yrast structures have been observed in the even-even,  $N = Z$  isotopes  $^{76}\text{Sr}$  and  $^{80}\text{Zr}$  [1, 2, 3]. The  $Z = 40$  and  $N = 40$  shell gaps appear to be more robust for neutron-rich nuclei. Both  $^{90}\text{Zr}_{50}$  and  $^{96}\text{Zr}_{56}$  exhibit features at low excitation energy that support the presence of a subshell gap at  $Z = 40$  [4, 5, 6]. This quasi-magic gap at  $Z = 40$  disappears with the addition of neutrons beyond  $N = 56$ , and such a behavior was attributed to the strong, attractive monopole interaction between  $1g_{9/2}$  protons and  $1g_{7/2}$  neutrons [7]. Evidence for magicity at  $N = 40$  for neutron-rich nuclei is gathered mainly from measurements on  $^{68}\text{Ni}_{40}$  and adjacent nuclei. The energy of the first  $2^+$  state [ $E(2_1^+)$ ] in  $^{68}\text{Ni}$  is 2033 keV [8], much higher than the  $E(2_1^+)$  values for the even-even neighbors  $^{66}\text{Ni}_{38}$  and  $^{70}\text{Ni}_{42}$ . The ratio  $E(4_1^+)/E(2_1^+)$  for the even-even Ni isotopes reaches a local minimum at  $^{68}\text{Ni}$ , another indication for added stability at  $Z = 28, N = 40$ . The low transition probability for excitation to the first  $2^+$  state in  $^{68}\text{Ni}$  [9, 10], relative to neighboring isotopes, is also in line with a double-magic character for this nucleus and the “goodness” of the subshell closure at  $N = 40$  for  $_{28}\text{Ni}$ .

However, it seems that the subshell gap at  $N = 40$  may be quickly reduced with the removal or addition of protons. As an example, the systematic variation of  $E(2_1^+)$  energies as a function of neutron number for the  $_{28}\text{Ni}$ ,  $_{26}\text{Fe}$ , and  $_{24}\text{Cr}$  isotopes is presented in Fig. 1. The  $E(2_1^+)$  values for the  $_{26}\text{Fe}$  and  $_{24}\text{Cr}$  isotopes decrease with increasing neutron number, even through  $N = 40$ . Hannawald *et al.* [11] identified the first  $2^+$  state in  $^{66}\text{Fe}_{40}$  from the  $\beta$  decay of  $^{66}\text{Mn}$ . The low value  $E(2_1^+) = 573$  keV was taken as an indication of possible collectivity near the ground state, and a deformation parameter  $\beta_2 = 0.26$  was deduced from the Grodzins relation [12]. The decreasing trend in  $E(2_1^+)$  values for the neutron-rich Fe isotopes continues in  $^{68}\text{Fe}_{42}$ , where the  $2_1^+$  level with energy 517 keV was identified by Adrich *et al.* [13] with in-beam  $\gamma$ -ray spectroscopy following  $2p$  knockout.

The systematic decrease in  $E(2_1^+)$  values is even more pronounced in the Cr isotopic chain (Fig. 1). Deformation parameters  $\beta_2 = 0.27$  and 0.31 have been deduced for the

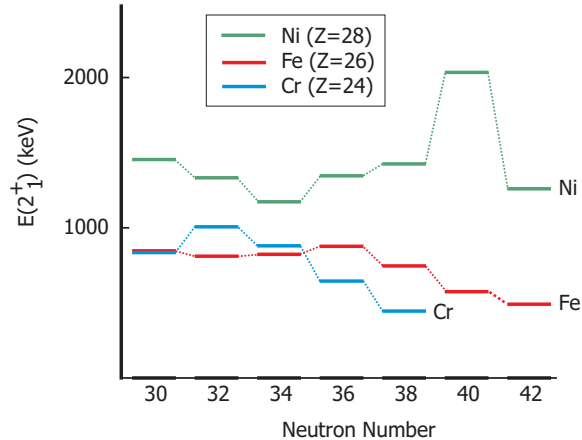


FIG. 1: (Color online) Systematic variation of  $E(2_1^+)$  for the even-even  $_{28}\text{Ni}$ ,  $_{26}\text{Fe}$  and  $_{24}\text{Cr}$  isotopes.

ground states of  $^{60}\text{Cr}_{36}$  and  $^{62}\text{Cr}_{38}$ , respectively [14], based on their  $E(2_1^+)$  values. Large quadrupole deformation lengths have also been reported for  $^{60,62}\text{Cr}$  based on results of proton inelastic scattering experiments [15, 16]. However, the medium-spin structure of  $^{60}\text{Cr}$  does not display features characteristic of a rotational pattern [17]. Although data for the low-energy structure of  $^{64}\text{Cr}_{40}$  are still lacking, the trend of a lowering of excitation energies for the neutron-rich  $_{24}\text{Cr}$  isotopes at and beyond  $N = 40$  is predicted [18].

The strength of the subshell closure at  $N = 40$  depends on the magnitude of the gap between the  $1f_{5/2}, 2p_{1/2}$  and  $1g_{9/2}$  neutron orbitals. The strong monopole interaction between protons in the  $1f_{7/2}$  shell and the neutrons in the  $1g_{9/2}$  orbital decreases when  $1f_{7/2}$  protons are removed, causing the narrowing of the  $1f_{5/2}-1g_{9/2}$  energy separation [11]. In addition, the first two Nilsson substates of the  $1g_{9/2}$  orbital are steeply downsloping with increasing deformation. Combined, these effects can create a situation in which the occupation of the deformed levels is energetically preferential to the occupation of the spherical states, leading to increased deformation and erosion of the  $N = 40$  subshell closure for  $Z < 28$ . The appearance of low-energy  $9/2^+$  states in the odd- $A$  Cr isotopes gives preliminary evidence that the  $1g_{9/2}$  neutron orbital is indeed nearing the Fermi surface. The rotational bands built on the  $9/2^+$  state in  $^{55}\text{Cr}_{31}$  [19] and  $^{57}\text{Cr}_{33}$  [20] suggest the presence of prolate-deformed structures. However, the isomeric nature of the  $9/2^+$  level in  $^{59}\text{Cr}_{35}$  [21] appears to be more indicative of modest oblate collectivity.

While the neutron-rich, even- $Z$   $_{26}\text{Fe}$  and  $_{24}\text{Cr}$  nuclei near  $N = 40$  have been investigated,

scant data are available regarding the level structures of the neighboring odd- $Z$   ${}_{25}\text{Mn}$ . The driving force leading to the lowering of the  $E(2_1^+)$  energies and possible onset of collectivity in the Cr and Fe isotopes near  $N = 40$  should be expected to act in a similar manner in the Mn nuclei. However, level structures are not available for Mn isotopes with  $N > 38$ . In-beam  $\gamma$  rays were recently measured for neutron-rich  ${}^{59-63}\text{Mn}$  produced by multi-nucleon transfer between a  ${}^{70}\text{Zn}$  projectile and  ${}^{238}\text{U}$  target [22]. Only a single  $\gamma$ -ray transition was attributed to  ${}^{63}\text{Mn}_{38}$ . Five  $\gamma$  rays were assigned to the low-energy structure of  ${}^{62}\text{Mn}_{37}$ , complementing the low-energy level scheme that had previously been proposed for this nucleus from  $\beta$  decay [23]. The low-energy structure of  ${}^{62}\text{Mn}$  is further complicated by the presence of two  $\beta$ -decaying states [23]. In-beam and  $\beta$ -delayed  $\gamma$  rays have likewise been assigned to  ${}^{61}\text{Mn}_{36}$ . However, no level scheme was proposed based on the five  $\beta$ -delayed  $\gamma$  rays reported by Sorlin *et al.* [24]. The low-energy structure of  ${}^{61}\text{Mn}$  offers an important opportunity to characterize further the possible onset of collectivity inferred from the systematic behavior of the even-even Cr and Fe isotopes. The decrease in  $E(2_1^+)$  values for neutron-rich Cr may suggest that deformation sets in at  ${}^{60}\text{Cr}$ , with  $N = 36$ , while evidence for such deformation effects in the Fe isotopes appears only at  ${}^{64}\text{Fe}$ , with  $N = 38$ .

Here, we report on the low-energy structure of  ${}^{61}\text{Mn}_{36}$ , populated following the  $\beta$  decay of  ${}^{61}\text{Cr}$ . We also examine the systematic variation of the low-energy level densities of the odd- $A$   ${}_{25}\text{Mn}$  isotopes and find no evidence for an early onset of collectivity at  $N = 36$ , as was proposed for neighboring  ${}_{24}\text{Cr}$  nuclei.

## II. EXPERIMENTAL PROCEDURE

The  $\beta$ -decay properties of  ${}^{61}\text{Cr}$  were studied at National Superconducting Cyclotron Laboratory (NSCL) at Michigan State University. A 130-MeV/nucleon  ${}^{76}\text{Ge}^{30+}$  beam was produced by the coupled cyclotrons at NSCL. The  ${}^{76}\text{Ge}$  primary beam was fragmented on a 47 mg/cm<sup>2</sup> Be target at the object position of the A1900 fragment separator [25]. The secondary fragments of interest were separated in the A1900 with a 300 mg/cm<sup>2</sup> Al wedge located at the intermediate image of the separator. The full momentum acceptance of the A1900 ( $\Delta p/p \sim 5\%$ ) was used for fragment collection.

Fragments were delivered to the  $\beta$ -decay experimental end station, which consisted of detectors from the Beta Counting System (BCS) [26] and the Segmented Germanium Array

(SeGA) [27]. A stack of 3 Si PIN detectors with thicknesses 991, 997 and 309  $\mu\text{m}$ , respectively, was placed upstream of the BCS and provided energy loss information for particle identification. Fragments were implanted in the 979  $\mu\text{m}$ -thick double-sided silicon microstrip detector (DSSD) of the BCS. This detector was segmented into 40 strips on both front and back, for a total of 1600 pixels. A total of  $1.32 \times 10^4$   $^{61}\text{Cr}$  ions was implanted into the DSSD over the course of the measurement. The particle identification spectrum is presented in Fig. 2.

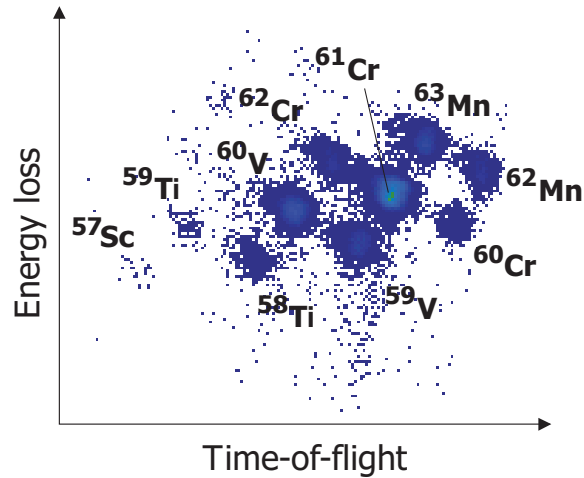


FIG. 2: (Color online) Particle identification plot measured at the experimental end station (BCS) for the A1900 magnetic rigidity setting  $B\rho_1 = 4.403$  Tm and  $B\rho_2 = 4.134$  Tm. Energy loss was measured in the most upstream PIN detector of the BCS. Time-of-flight was deduced from the difference in timing signals of the same PIN detector and a plastic scintillator at the intermediate image of the A1900. An event-by-event momentum correction of the time-of-flight was performed based on the position information obtained from the plastic scintillator.

Delayed  $\gamma$  rays were detected by 16 Ge detectors from SeGA, arranged in two concentric circles around the BCS detectors. The  $\gamma$ -ray peak detection efficiency varied from 20% at 100 keV to 7% at 1 MeV. The energy resolution of each Ge detector was measured to be better than 3.5 keV for the 1.3-MeV  $\gamma$  ray in  $^{60}\text{Co}$ .

### III. RESULTS

Implanted  $^{61}\text{Cr}$  fragments were correlated with their subsequent  $\beta$  decays by requiring the presence of a high-energy implantation event in a single pixel of the DSSD, followed by a low-energy  $\beta$  event in the same or any of the eight neighboring pixels. The decay curve for  $^{61}\text{Cr}$ -correlated  $\beta$  decays given in Fig. 3 was generated by histogramming the differences between absolute time stamps for implantation and correlated decay events. The curve was fitted with a single exponential decay combined with an exponential growth and decay of the short-lived daughter,  $^{61}\text{Mn}$ , whose half-life was taken to be  $670 \pm 40$  ms as adopted in Ref. [28]. A constant background was also included as a free parameter in the fit. A half-life of  $233 \pm 11$  ms was deduced for the ground-state  $\beta$  decay of  $^{61}\text{Cr}$ . This new value compares favorably with a previous measurement by Sorlin *et al.* [24] of  $251 \pm 22$  ms, but is more than  $1\sigma$  shorter than the  $270 \pm 20$  ms value deduced earlier by Ameil *et al.* [29].

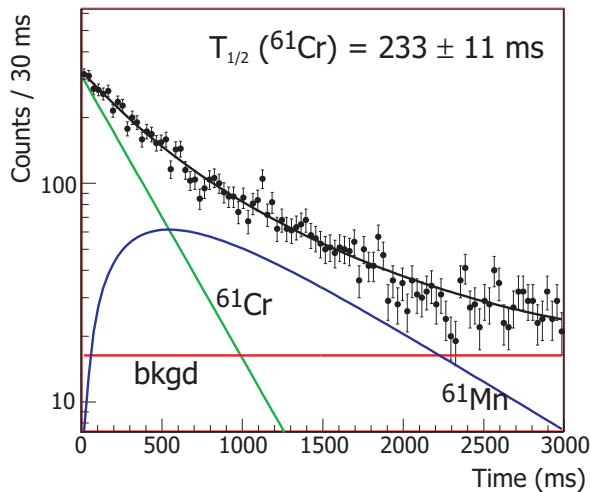


FIG. 3: (Color online) Decay curve for  $^{61}\text{Cr}$ , based on fragment- $\beta$  correlations. Data were fitted with a single exponential decay and exponential growth and decay of the short-lived daughter,  $^{61}\text{Mn}$  ( $T_{1/2} = 670 \pm 40$  ms). A constant background was also considered in the fit.

The  $\beta$ -delayed  $\gamma$ -ray spectrum for the decay of  $^{61}\text{Cr}$  is shown in Fig. 4. The spectrum covers the energy range 0 to 2.5 MeV, and the observed  $\gamma$  rays correspond to events that occurred within the first 3 s following a  $^{61}\text{Cr}$  implantation. Seven transitions have been assigned to the decay of  $^{61}\text{Cr}$  and are listed in Table I. The peaks observed with energies of 207 and 629 keV in Fig. 4 are known transitions in the decay of the  $^{61}\text{Mn}$  daughter [30]. The

1028- and 1205-keV transitions in the decay of the grand-daughter  $^{61}\text{Fe}$  [31] are also seen in Fig. 4. The peaks at 355, 535, 1142 and 1861 keV correspond in energy to the transitions previously observed with low statistics by Sorlin *et al.* [24]. However, the transition observed in Ref. [24] at 1134 keV was not apparent in the spectrum of Fig. 4. The three additional  $\gamma$ -ray transitions at 157, 1497, and 2378 keV are assigned for the first time to the decay of  $^{61}\text{Cr}$ . Coincidentally, two transitions with energies 155 and 355 keV had previously been assigned to the  $\beta$  decay of  $^{62}\text{Cr}$  [23]. Observation of these transitions in Fig. 4 suggests that they are associated with levels in  $^{61}\text{Mn}$ , and their observation in Ref. [23] may be evidence for  $\beta$ -delayed neutron decay of the  $^{62}\text{Cr}$  ground state. It is worth noting that the in-beam  $\gamma$ -ray spectra for  $^{61}\text{Mn}$  and  $^{62}\text{Mn}$  obtained by Valiente-Dobón *et al.* [22] include transitions of energies 157 and 155 keV, respectively, supporting the present assignment of the 157-keV  $\gamma$ -ray transition in Fig. 4 to the decay of  $^{61}\text{Cr}$ .

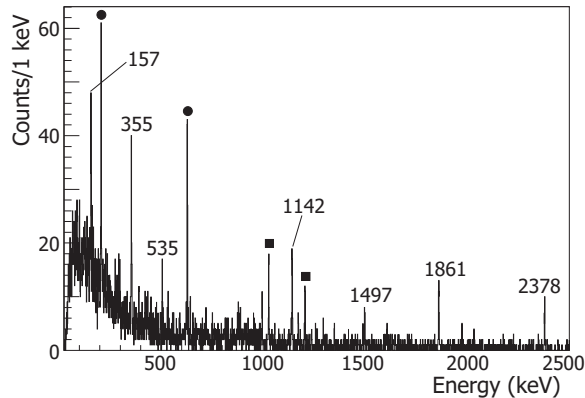


FIG. 4:  $\beta$ -delayed  $\gamma$  rays following the decay of  $^{61}\text{Cr}$ . Known  $\gamma$  rays from the decay of the daughter  $^{61}\text{Mn}$  and the granddaughter  $^{61}\text{Fe}$  are indicated by the filled circles and squares, respectively. Transitions assigned to the decay of  $^{61}\text{Cr}$  are marked by their energy in keV.

The proposed decay scheme for levels in  $^{61}\text{Mn}$  populated following the  $\beta$  decay of  $^{61}\text{Cr}$  is presented in Fig. 5. The  $\beta$ -decay  $Q$  value was taken from Ref. [32]. Absolute  $\gamma$ -ray intensities were deduced from the number of observed  $^{61}\text{Cr}$   $\gamma$  rays, the  $\gamma$ -ray peak efficiency, and the number of  $^{61}\text{Cr}$  implants correlated with  $\beta$  decays, as derived from the fit of the decay curve in Fig. 3. The two- $\gamma$  cascade involving the 1142- and 355-keV transitions was confirmed by  $\gamma\gamma$  coincidence relationships (see Fig. 6). However, the ordering of the two transitions is not uniquely determined. The arrangement of Fig. 5 was based on the absolute intensities

TABLE I: Energies and absolute intensities of delayed  $\gamma$  rays assigned to the decay of  $^{61}\text{Cr}$ . The initial and final states for those transitions placed in the proposed  $^{61}\text{Mn}$  level scheme of Fig. 5 are also indicated.

$E_\gamma$	$I_\gamma^{abs}$	$E_{initial}$ (keV)	$E_{final}$ (keV)	Coincident $\gamma$ rays (keV)
$157.2 \pm 0.5$	$9 \pm 2$	157	0	
$354.8 \pm 0.4$	$16 \pm 2$	1497	1142	535, 1142
$534.6 \pm 0.5$	$5 \pm 1$	2032	1497	355
$1142.2 \pm 0.4$	$21 \pm 2$	1142	0	355
$1497.3 \pm 0.5$	$9 \pm 2$	1497	0	
$1860.8 \pm 0.4$	$20 \pm 2$	1861	0	
$2378.2 \pm 0.4$	$11 \pm 1$	2378	0	

of the 1142- and 355-keV transitions. No evidence was found for  $\gamma$  rays in coincidence with the 157-keV ground-state transition within the statistical uncertainty of the measurement. Two counts in the 355-keV coincidence spectrum of Fig. 6(b) suggested placement of the 535-keV line in cascade from a higher-lying level at 2032 keV. This tentative placement is represented in Fig. 5 by a dashed line.

Apparent  $\beta$ -decay feeding to levels in  $^{61}\text{Mn}$  was deduced from the absolute  $\gamma$ -ray intensities. The deduced values, along with apparent  $\log ft$  values, are also given in Fig. 5. The observed  $\beta$  branches all have apparent  $\log ft$  values between 4 and 6, consistent with allowed transitions. The 1142-keV level is deduced to have a small  $\beta$  branching with a large error, and may not be directly populated by the  $\beta$  decay of  $^{61}\text{Cr}$ .

A ground-state spin and parity assignment of  $5/2^-$  was adopted for  $^{61}\text{Mn}$ , by Runte *et al.* [30], based on the systematic trends of ground state  $J^\pi$  values for the less neutron-rich, odd- $A$  Mn isotopes. The first excited state at 157 keV has been tentatively assigned  $J^\pi = 7/2^-$  from the in-beam  $\gamma$ -ray results [22]. Allowed  $\beta$  feeding to the lowest two states would then limit the  $J^\pi$  quantum numbers of the  $^{61}\text{Cr}$  ground state to values of  $5/2^-$  or  $7/2^-$ . Gaudefroy *et al.* [23] tentatively assigned  $J^\pi = 5/2^-$  to the ground state of  $^{61}\text{Cr}$  on the basis of the observed  $\beta$ -decay properties of the progenitor,  $^{61}\text{V}$ , and such an assignment is adopted in Fig. 5. It is likely that the 1142-keV state has low spin, either  $J^\pi = 1/2^-$  or  $J^\pi = 3/2^-$ .

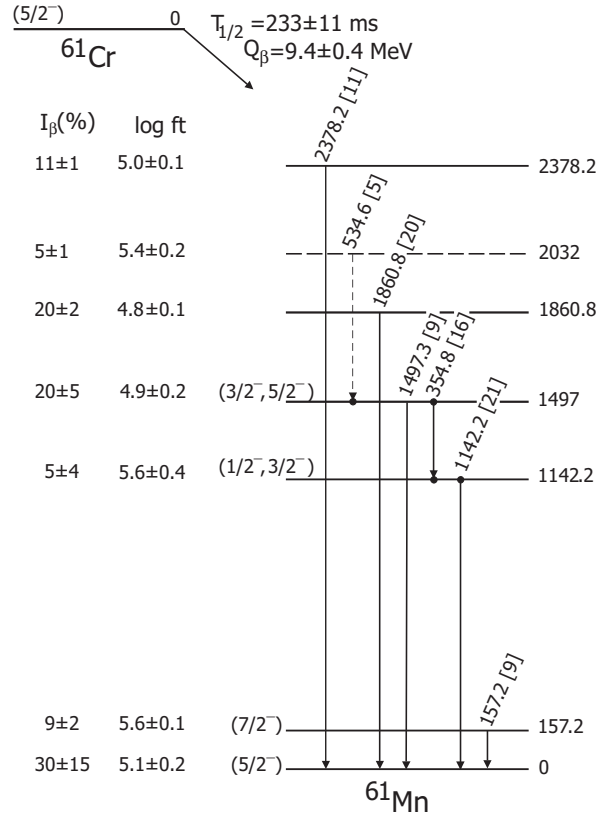


FIG. 5: Proposed  $^{61}\text{Mn}$  level scheme populated following the  $\beta$  decay of  $^{61}\text{Cr}$ . The number in brackets following a transition energy is the absolute  $\gamma$ -ray intensity. The  $Q$  value was taken from Ref. [32]. Observed coincidences are represented by filled circles. Absolute  $\beta$ -decay intensities and apparent log  $ft$  values to each state in  $^{61}\text{Mn}$  are given on the left-hand side of the figure. The dashed state at 2032 keV is tentatively placed as described in the text.

The level at 1142 keV is apparently weakly fed by  $\beta$  decay, was not identified in the yrast structure of  $^{61}\text{Mn}$  [22], and does not depopulate to the  $7/2^-$  level at 157 keV within the statistical certainty of this measurement. The 1497-keV level is tentatively assigned a  $J^\pi$  of  $3/2^-$  or  $5/2^-$  because of the apparent allowed  $\beta$ -decay branch and the favorable competition between the two depopulating  $\gamma$  rays that suggests both transitions have M1 multipolarity. The proposed levels at excitation energies of 1861 and 2378 keV are apparently fed by allowed  $\beta$  decay as well, and can take  $J^\pi$  values in a range from  $3/2^-$  to  $7/2^-$ .

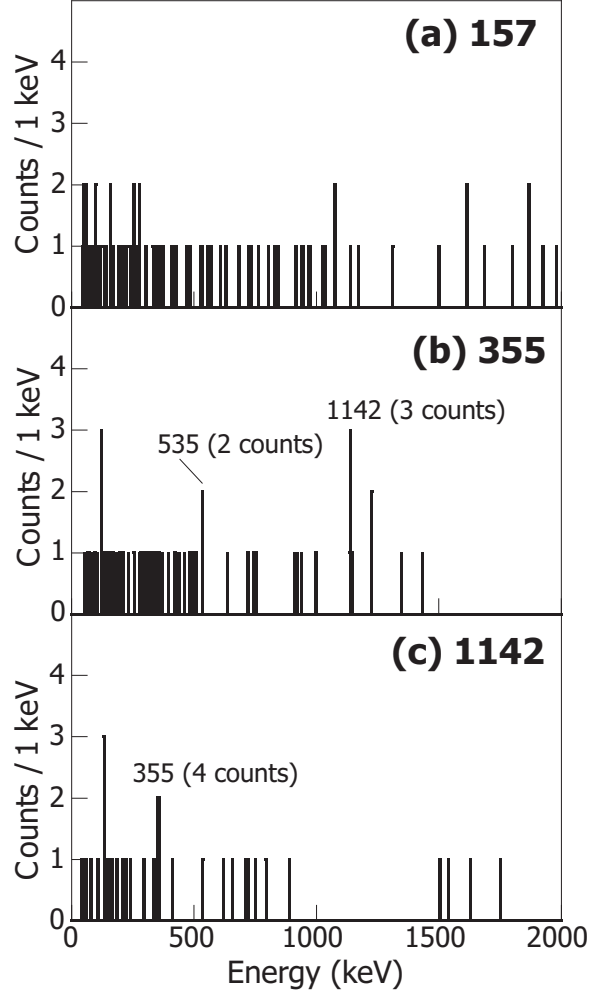


FIG. 6:  $\gamma\gamma$  coincidence spectra for: (a) 157 keV; (b) 355 keV; and (c) 1142 keV  $\gamma$  rays. The spikes observed below 200 keV in (b) and (c) represent 3 counts each in a single channel at low energy, and an absence of width uncharacteristic of a true  $\gamma$ -ray coincidence.

#### IV. DISCUSSION

The possible increase in collectivity inferred at low energy for the neutron-rich  ${}_{24}\text{Cr}$  and  ${}_{26}\text{Fe}$  isotopes has been associated with the presence of the neutron  $1g_{9/2}$  single-particle orbital near the Fermi surface as  $N = 40$  is approached. As noted in the introduction, the systematic variation in  $E(2_1^+)$  values (Fig. 1) may suggest that deformation sets in already at  $N = 36$  for the Cr isotopes, while first evidence for such deformation effects in the Fe isotopes occurs at  ${}^{64}\text{Fe}$ , which has  $N = 38$ . Therefore, it could be speculated that the low-energy structure of  ${}^{61}\text{Mn}$ , with  $N = 36$ , might already exhibit features at low energy

suggestive of a change in collectivity when compared to other odd- $A$  Mn isotopes nearer to stability.

### A. Odd- $A$ Mn Isotopes

The systematics of the known energy levels of the odd- $A$  Mn isotopes with  $A = 57 - 63$  can be found in Fig. 7. The levels shown below 2 MeV for  $^{57}\text{Mn}$  are taken from  $\beta$  decay of  $^{57}\text{Cr}$  [33], in-beam  $\gamma$ -ray spectroscopy [34], and the  $(d, ^3\text{He})$  transfer reaction [35].  $\beta$  decay apparently populates seven excited states below 2 MeV, as well as the  $^{57}\text{Mn}$  ground state. The states directly fed by  $\beta$  decay are all assumed to have negative parity, since the  $^{57}\text{Cr}$  parent has ground state  $J^\pi = 3/2^-$  quantum numbers. The negative parity yrast states observed in  $^{57}\text{Mn}$  were populated by a heavy-ion induced fusion-evaporation reaction, and resulted in tentative spin assignments to levels up to  $J = 25/2$ . The  $(d, ^3\text{He})$  transfer reaction provided unambiguous  $J^\pi$  assignments to the negative parity states below 2 MeV at 84, 851, and 1837 keV, based on angular distribution data. Positive parity was deduced for the excited states with energies 1753 and 1965 keV. Based on the spectroscopic strengths for proton pickup [35], the first  $7/2^-$ ,  $1/2^+$ , and  $3/2^+$  levels in  $^{57}\text{Mn}$  were deduced to carry  $\sim 40\%$  of the summed single-particle strength from shell model expectations.

Valiente-Dobón *et al.* [22] studied neutron-rich Mn isotopes by in-beam  $\gamma$ -ray spectroscopy following deep inelastic collisions of a  $^{70}\text{Zn}$  beam on a  $^{238}\text{U}$  target. Negative-parity yrast states were identified up to  $J = 15/2$  in  $^{59}\text{Mn}_{34}$  and  $J = 11/2$  in  $^{61}\text{Mn}_{36}$ . Only a single transition, with energy 248 keV, was assigned to the structure of  $^{63}\text{Mn}_{38}$ . The non-yrast levels in  $^{59,61}\text{Mn}$  shown in Fig. 7 were identified following  $\beta$  decay. The  $\beta$  decay of  $^{59}\text{Cr}$  to levels in  $^{59}\text{Mn}$  was most recently reported by Liddick *et al.* [36]. The ground state spin and parity of the parent  $^{59}\text{Cr}$ , tentatively assigned as  $J^\pi = 1/2^-$ , restricts the range of states in  $^{59}\text{Mn}$  accessible by allowed  $\beta$  decay to those with  $J^\pi = 1/2^-, 3/2^-$ . The ground state of  $^{59}\text{Mn}$  is known to have  $J^\pi = 5/2^-$  [37]. The non-yrast  $J^\pi$  values for  $^{59}\text{Mn}$  were inferred from the  $\beta$ - and  $\gamma$ -decay patterns.

The negative parity yrast structures below 2 MeV in odd- $A$   $^{57,59,61}\text{Mn}$  exhibit little variation as a function of neutron number. These levels are consistent with shell model calculations reported in Ref. [22] employing the GXPF1A, KB3G and *fpg* effective interactions. The authors of Ref. [22] do note, however, that the proper ordering of the  $9/2^-$  and  $11/2^-$

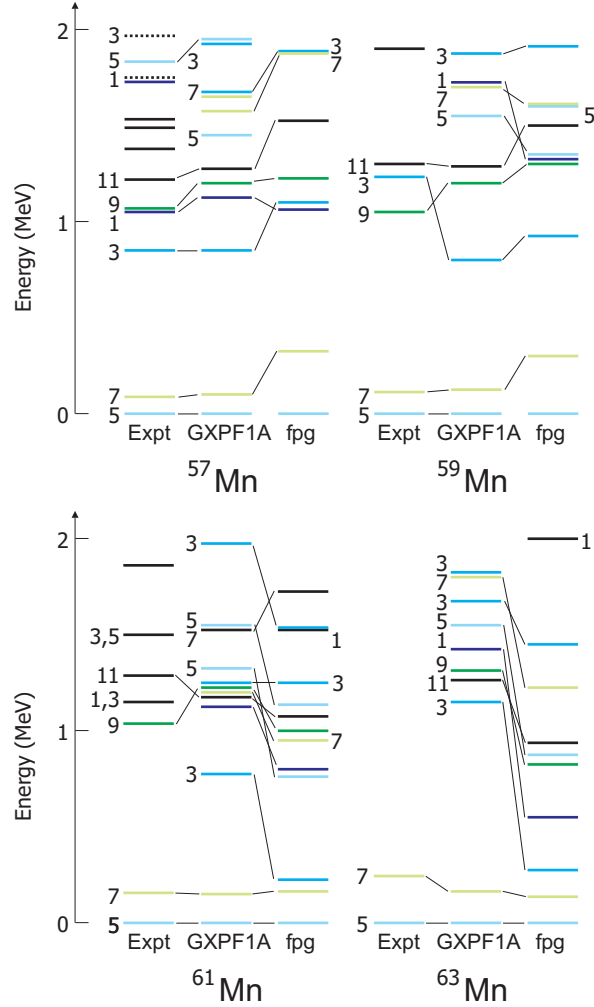


FIG. 7: (Color online) Systematic variation of the low-energy levels of the neutron-rich, odd- $A$   $^{25}\text{Mn}$  isotopes, along with the results of shell model calculations with the GXPF1A and  $fpg$  interactions. Only levels below 2 MeV are presented. In addition, the shell model results shown are limited to the three lowest energy levels calculated for  $J^\pi = 1/2^- - 7/2^-$ , and the yrast levels for  $J^\pi = 9/2^-$  and  $11/2^-$ . Levels with assumed negative parity are shown as solid lines, and those with positive parity are presented as dotted lines. Spins are given as  $2I$  and, in nearly all cases, are tentative as discussed in the text.

levels at  $\sim 1$  MeV is reproduced for all three isotopes only by the  $fpg$  interaction. The experimental energy gap between the ground state, with  $J^\pi = 5/2^-$ , and the  $7/2^-$  first excited state exhibits a regular increase from  $^{57}\text{Mn}$  (83 keV) to  $^{65}\text{Mn}$  (272 keV) [23]. Both the GXPF1A and  $fpg$  shell model interactions reproduce the observed trends well.

The shell model calculations in Ref. [22] were extended to include non-yrast states below 2 MeV. The calculations were performed with the code ANTOINE [38] and the GXPF1A [39] and  $fp$  [9] effective interactions. The full  $fp$  model space was utilized for the calculations with the GXPF1A interaction. The valence space for the calculations with the cross shell interaction  $fp$  was limited to 2 neutron excitations from the  $fp$  shell to the  $1g_{9/2}$  orbital. As compared to Ref. [22], the truncation of the basis was necessary to reach convergence for the higher density of states at lower spin for the most neutron-rich Mn isotopes considered here. However, in those cases where the calculations were completed with both 2 and 6 neutron excitations allowed from the  $fp$  shell, similar results were obtained.

The low density of levels below 1 MeV is persistent in  $^{57,59,61}\text{Mn}$ , and follows the shell model results with the GXPF1A effective interaction well. The only excited state in this energy range is the  $7/2^-$  level, which is expected to carry a reduced  $1f_{7/2}$  single-particle component with the addition of neutrons [35]. The low-spin level density below 1 MeV is shown to increase at  $^{61}\text{Mn}$  in the shell model results with the  $fp$  interaction. Here, the influence of the  $1g_{9/2}$  neutron orbital becomes apparent at  $N = 36$ . However, this is not borne out in the observed level structure. The regular behavior of the low-energy levels of the odd- $A$   $_{25}\text{Mn}$  isotopes through  $N = 36$  follows the similar trend observed in the even-even  $_{26}\text{Fe}$  isotopes, where the possible onset of collectivity at low energy is not evident until  $N = 38$  is reached.

## B. Even- $A$ Mn Isotopes

Although the present experiment did not report any new information on even- $A$  Mn isotopes, for the sake of completeness we include them in the discussion. Only a few excited states in the odd-odd  $^{60,62}\text{Mn}$  are established, based on  $\beta$ -decay studies. Two  $\beta$ -decaying states are known in both isotopes, but the location and ordering of the proposed  $1^+$  and  $4^+$  states is not established in  $^{62}\text{Mn}_{37}$  [23]. Good agreement was noted between shell model results with the GXPF1 interaction and both the low-energy structure and  $\beta$ -decay properties of  $^{60}\text{Mn}_{35}$  [40]. The low-energy structure of  $^{62}\text{Mn}$  built on the  $1^+$   $\beta$ -decaying state shows marked similarity to that in  $^{60}\text{Mn}$ , albeit the excited  $2^+$  and  $1^+$  states are both shifted  $\sim 100$  keV lower in energy with the addition of two neutrons. Although Valiente-Dobón *et al.* reported a number of in-beam  $\gamma$  rays associated with the depopulation of yrast levels in

both  $^{60}\text{Mn}$  and  $^{62}\text{Mn}$ , no level structures were proposed due to the lack of coincidence data in the literature [22]. A key feature yet to be identified in the neutron-rich, odd-odd Mn isotopes is the location of the negative-parity levels that could signify the presence of the intruding  $1g_{9/2}$  neutron orbital. Again, the systematic variation of the (few) excited levels established in the odd-odd Mn isotopes through  $N = 37$  does not suggest a sudden onset of collectivity, in line with the trend established for the yrast states of even-even  $_{26}\text{Fe}$  isotopes.

## V. SUMMARY

The  $\beta$  decay of  $^{61}\text{Cr}$  has been studied to extract details on non-yrast excited states in the daughter nucleus  $^{61}\text{Mn}$ . A more accurate half-life of  $233 \pm 11$  ms was deduced for the ground-state of  $^{61}\text{Cr}$ , consistent with the previous measurement by Sorlin *et al.* [24]. The low-energy level scheme for  $^{61}\text{Mn}$ , deduced following  $\beta$  decay of  $^{61}\text{Cr}$ , features five new excited states above a 1-MeV excitation energy. However, the low-energy structure below 1 MeV does not resemble that expected from the shell model results that consider the  $1g_{9/2}$  orbital. The low density of states below 1 MeV is a consistent feature observed in the odd- $A$  Mn isotopes with  $A = 57, 59, 61$ , and follows the results of shell model calculations in the  $fp$  model space, without a need to invoke neutron excitations into the  $1g_{9/2}$  orbital. There is also little variation in the yrast structures of these odd- $A$  Mn isotopes up to  $J = 15/2$ , as reported by Valiente-Dobón *et al.* [22]. No compelling evidence was found for a possible onset of collectivity in the low-energy structures of the Mn isotopes through  $N = 37$ . This observation is consistent with the behavior of the even-even,  $Z + 1$   $_{26}\text{Fe}$  isotopes, but not with that of the even-even  $Z - 1$   $_{24}\text{Cr}$  isotopes, where possible onset of collectivity at low energy has been suggested from the  $E(2_1^+)$  energy at  $N = 36$ . Scant data are available for both yrast and non-yrast levels in the  $_{25}\text{Mn}$  isotopes beyond  $N = 36$ . Such data will be critical to evaluate the role of the neutron  $1g_{9/2}$  orbital in defining the structural properties of the neutron-rich Mn isotopes.

## Acknowledgments

The authors thank the NSCL operations staff for providing the primary and secondary beams for this experiment and the NSCL  $\gamma$  group for assistance in setting up the Ge detectors

from SeGA. This work was supported in part by the National Science Foundation Grant No. PHY-06-06007, the U.S. Department of Energy, Office of Nuclear Physics, under contracts DE-AC02-06CH11357 and DE-FG02-94ER40834, and the Polish Academy of Sciences grant 1PO3B 059 29. HLC acknowledges support from the Natural Science and Engineering Research Council (NSERC) of Canada.

---

- [1] C.J. Lister, P.J. Ennis, A.A. Chishti, B.J. Varley, W. Gelletly, H.G. Price, and A.N. James, *Phys. Rev. C* **42**, R1191 (1990).
- [2] C.J. Lister, M. Campbell, A.A. Chishti, W. Gelletly, L. Goettig, R. Moscrop, B.J. Varley, A.N. James, T. Morrison, H.G. Price, J. Simpson, K. Connel, and O Skeppstedt, *Phys. Rev. Lett.* **59**, 1270 (1987).
- [3] S.M. Fischer, C.J. Lister, D.P. Balamuth, R. Bauer, J.A. Becker, L.A. Bernstein, M.P. Carpenter, J. Durell, N. Fotiades, S.J. Freeman, P.E. Garrett, P.A. Hausladen, R.V.F. Janssens, D. Jenkins, M. Leddy, J. Ressler, J. Schwartz, D. Svelnys, D.G. Sarantites, D. Seweryniak, B.J. Varley, and R. Wyss, *Phys. Rev. Lett.* **87**, 132501 (2001).
- [4] N. Auerbach and I. Talmi, *Nucl. Phys.* **64**, 458 (1965).
- [5] D. Gloeckner, *Nucl. Phys.* **A253**, 301 (1975).
- [6] P. Federman, S. Pittel, and R. Campos, *Phys. Lett.* **82B**, 9 (1979).
- [7] P. Federman and S. Pittel, *Phys. Lett.* **69B**, 385 (1977).
- [8] R. Broda, B. Fornal, W. Królas, T. Pawlat, D. Bazzacco, S. Lunardi, C. Rossi-Alvarez, R. Menegazzo, G. de Angelis, P. Bednarczyk, J. Rico, D. De Acuña, P.J. Daly, R.H. Mayer, M. Sferrazza, H. Grawe, K.H. Maier, and R. Schubart, *Phys. Rev. Lett.* **74**, 868 (1995).
- [9] O. Sorlin, S. Leenhardt, C. Donzaud, J. Duprat, F. Azaiez, F. Nowacki, H. Grawe, Zs. Dombrádi, F. Amorini, A. Astier, D. Baiborodin, M. Belleguic, C. Borcea, C. Bourgeois, D.M. Cullen, Z. Dlouhy, E. Dragulescu, M. Górska, S. Grévy, D. Guillemaud-Mueller, G. Hagemann, B. Herskind, J. Kiener, R. Lemmon, M. Lewitowicz, S.M. Lukyanov, P. Mayet, F. de Oliveira Santos, D. Pantalica, Yu.-E. Penionzhkevich, F. Pougheon, A. Poves, N. Redon, M.G. Saint-Laurent, J.A. Scarpaci, G. Sletten, M. Stanoiu, O. Tarasov, and Ch. Theisen, *Phys. Rev. Lett.* **88**, 092501 (2002).
- [10] N. Bree, I. Stefanescu, P.A. Butler, J. Cederkäll, T. Davinson, P. Delahaye, J. Eberth, D. Fe-

- dorov, V.N. Fedosseev, L.M. Fraile, S. Franchoo, G. Georgiev, K. Gladnishki, M. Huyse, O. Ivanov, J. Iwanicki, J. Jolie, U. Köster, Th. Kröll, R. Krücken, B.A. Marsh, O. Niedermaier, P. Reiter, H. Scheit, D. Schwalm, T. Sieber, J. Van de Walle, P. Van Duppen, N. Warr, D. Weisshaar, F. Wenander, and S. Zemlyanoy, *Phys. Rev. C* **78**, 047301 (2008).
- [11] M. Hannawald, T. Kautzsch, A. Wöhr, W.B. Walters, K.-L. Kratz, V.N. Fedoseyev, V.I. Mishin, W. Böhmer, B. Pfeiffer, V. Sebastian, Y. Jading, U. Köster, J. Lettry, H.L. Ravn and the ISOLDE Collaboration, *Phys. Rev. Lett.* **82**, 1391 (1999).
- [12] L. Grodzins, *Phys. Lett.* **2**, 88 (1962).
- [13] P. Adrich, A.M. Amthor, D. Bazin, M.D. Bowen, B.A. Brown, C.M. Campbell, J.M. Cook, A. Gade, D. Galaviz, T. Glasmacher, S. McDaniel, D. Miller, A. Obertelli, Y. Shimbara, K.P. Siwek, J.A. Tostevin, and D. Weisshaar, *Phys. Rev. C* **77**, 054306 (2008).
- [14] O. Sorlin, C. Donzaud, F. Nowacki, J.C. Angélique, F. Azaiez, C. Bourgeois, V. Chiste, Z. Dlouhy, S. Grévy, D. Guillemaud-Mueller, F. Ibrahim, K.-L. Kratz, M. Lewitowicz, S.M. Lukyanov, J. Mrasek, Yu.-E. Penionzhkevich, F. de Oliveira Santos, B. Pfeiffer, F. Pougheon, A. Poves, M.G. Saint-Laurent, and M. Stanoiu, *Eur. Phys. J. A* **16**, 55 (2003).
- [15] N. Aoi, H. Suzuki, E. Takeshita, S. Takeuchi, S. Ota, H. Baba, S. Bishop, T. Fukui, Y. Hashimoto, H.J. Ong, E. Ideguchi, K. Ieki, N. Imai, H. Iwaski, S. Kanno, Y. Kondo, T. Kubo, K. Kurita, K. Kusaka, T. Minemura, T. Motobayashi, T. Nakabayashi, T. Nakamura, T. Nakao, M. Niikura, T. Okumura, T.K. Ohniski, H. Sakurai, S. Shimoura, R. Sugo, D. Suzuki, M.K. Suzuki, M. Tamaki, K. Tanaka, Y. Togano, and K. Yamada, *Nucl. Phys.* **A805**, 400c (2008).
- [16] N. Aoi, E. Takeshita, H. Suzuki, S. Takeuchi, S. Ota, H. Baba, S. Bishop, T. Fukui, Y. Hashimoto, H.J. Ong, E. Ideguchi, K. Ieki, N. Imai, M. Ishihara, H. Iwasaki, S. Kanno, Y. Kondo, T. Kubo, K. Kurita, K. Kusaka, T. Minemura, T. Motobayashi, T. Nakabayashi, T. Nakamura, T. Nakao, M. Niikura, T. Okumura, T.K. Ohnishi, H. Sakurai, S. Shimoura, R. Sugo, D. Suzuki, M.K. Suzuki, M. Tamaki, K. Tanaka, Y. Togano, and K. Yamada, *Phys. Rev. Lett.* **102**, 012502 (2009).
- [17] S. Zhu, A.N. Deacon, S.J. Freeman, R.V.F. Janssens, B. Fornal, M. Honma, F.R. Xu, R. Broda, I.R. Calderin, M.P. Carpenter, P. Chowdhury, F.G. Kondev, W. Królas, T. Lauritsen, S.N. Liddick, C.J. Lister, P.F. Mantica, T. Pawlat, D. Seweryniak, J.F. Smith, S.L. Tabor, B.E. Tomlin, B.J. Varley and J. Wrzesiński, *Phys. Rev. C* **74**, 064315 (2006).

- [18] K. Kaneko, Y. Sun, M. Hasegawa, and T. Mizusaki, *Phys. Rev. C* **78**, 064312 (2008).
- [19] D.E. Appelbe, C.J. Barton, M.H. Muikku, J. Simpson, D.D. Warner, C.W. Beausang, M.A. Caprio, J.R. Cooper, J.R. Novak, N.V. Zamfir, R.A.E. Austin, J.A. Cameron, C. Malcolmson, J.C. Waddington, and F.R. Xu, *Phys. Rev. C* **67**, 034309 (2003).
- [20] A.N. Deacon, S.J. Freeman, R.V.F. Janssens, F.R. Xu, M.P. Carpenter, I.R. Calderin, P. Chowdhury, N.J. Hammond, T. Lauritsen, C.J. Lister, D. Seweryniak, J.F. Smith, S.L. Tabor, B.J. Varley, and S. Zhu, *Phys. Lett. B* **622**, 151 (2005).
- [21] S.J. Freeman, R.V.F. Janssens, B.A. Brown, M.P. Carpenter, S.M. Fischer, N.J. Hammond, M. Honma, T. Lauritsen, C.J. Lister, T.L. Khoo, G. Mukherjee, D. Seweryniak, J.F. Smith, B.J. Varley, M. Whitehead, and S. Zhu, *Phys. Rev. C* **69**, 064301 (2004).
- [22] J.J. Valiente-Dobón, S.M. Lenzi, S.J. Freeman, S. Lunardi, J.F. Smith, A. Gottardo, F. Della Vedova, E. Farnea, A. Gadea, D.R. Napoli, M. Axiotis, S. Aydin, D. Bazzacco, P.G. Bizzeti, A.M. Bizzeti-Sona, G. Benzoni, D. Bucurescu, L. Corradi, A.N. Deacon, G. de Angelis, E. Fioretto, B. Guiot, M. Ionescu-Bujor, A. Iordachescu, S. Leoni, N. Mărginean, R. Mărginean, P. Mason, R. Menegazzo, D. Mengoni, B. Million, G. Montagnoli, R. Orlandi, F. Recchia, E. Sahin, F. Scarlassara, R.P. Singh, A.M. Stefanini, D. Steppenbeck, S. Szilner, C.A. Ur, B.J. Varley, and O. Wieland, *Phys. Rev. C* **78**, 024302 (2008).
- [23] L. Gaudefroy, O. Sorlin, C. Donzaud, J.C. Angélique, F. Azaiez, C. Bourgeois, V. Chiste, Z. Dlouhy, S. Grévy, D. Guillemaud-Mueller, F. Ibrahim, K.-L. Kratz, M. Lewitowicz, S.M. Lukyanov, I. Matea, J. Mrasek, F. Nowacki, F. de Oliveira-Santos, Yu.-E. Penionzhkevich, B. Pfeiffer, F. Pougheon, M.G. Saint-Laurent, and M. Stanoiu, *Eur. Phys. J. A* **23**, 41 (2005).
- [24] O. Sorlin, C. Donzaud, L. Axelsson, M. Belleguic, R. Béraud, C. Borcea, G. Canchel, E. Chabanat, J.M. Daugas, A. Emsallem, M. Girod, D. Guillemaud-Mueller, K.-L. Kratz, S. Leenhardt, M. Lewitowicz, C. Longour, M.J. Lopez, F. de Oliveira Santos, L. Petizon, B. Pfeiffer, F. Pougheon, M.G. Saint-Laurent, and J.E. Sauvestre, *Nucl. Phys.* **A669**, 351 (2000).
- [25] D.J. Morrissey, B.M. Sherrill, M. Steiner, A. Stolz, and I. Wiedenhöver, *Nucl. Instrum. Methods Phys. Res. B* **204**, 90 (2003).
- [26] J.I. Prisciandaro, A.C. Morton, and P.F. Mantica, *Nucl. Instrum. Methods Phys. Res. A* **505**, 140 (2003).
- [27] W.F. Mueller, J.A. Church, T. Glasmacher, D. Gutknecht, G. Hackman, P.G. Hansen, Z. Hu,

- K.L. Miller, and P. Quirin, Nucl. Instrum. Methods Phys. Res. A **466**, 492 (2001).
- [28] M.R. Bhat, Nucl. Data Sheets **88**, 417 (1999).
- [29] F. Ameil, M. Bernas, P. Armbruster, S. Czajkowski, Ph. Dessagne, H. Geissel, E. Hanelt, C. Kozhuharov, C. Miede, C. Donzaud, A. Grewe, A. Heinz, Z. Janas, M. de Jong, W. Schwab, and S. Steinhäuser, Eur. Phys. J. A **1**, 275 (1998).
- [30] E. Runte, K.-L. Gippert, W.-D. Schmidt-Ott, P. Tidemand-Petersson, L. Ziegeler, R. Kirchner, O. Klepper, P.O. Larsson, E. Roeckl, D. Schardt, N. Kaffrell, P. Peuser, M. Bernas, Ph. Dessagne, M. Langevin, and K. Rykaczewski, Nucl. Phys. **A441**, 237 (1985).
- [31] J. Bron, H.W. Jongsma, and H. Verheul, Phys. Rev. C **11**, 966 (1975).
- [32] G. Audi, A.H. Wapstra, and C. Thibault, Nucl. Phys. **A729**, 337 (2003).
- [33] C.N. Davids, D.F. Geesaman, S.L. Tabor, M.J. Murphy, E.B. Norman, and R.C. Pardo, Phys. Rev. C **17**, 1815 (1978).
- [34] D.E. Appelbe, R.A.E. Austin, G.C. Ball, J.A. Cameron, B. Djerroud, T.E. Drake, S. Flibotte, C.D. O'Leary, A. Melarangi, C.E. Svensson, J.C. Waddington, and D. Ward, Eur. Phys. J. A **8**, 153 (2000).
- [35] N.G. Puttaswamy, W. Oelert, A. Djalois, C. Mayer-Böricke, P. Turek, P.W.M. Glaudemans, B.C. Metsch, K. Heyde, M. Waroquier, P. van Isaker, G. Wenes, V. Lopac, and V. Paar, Nucl. Phys. **A 401**, 269 (1983).
- [36] S.N. Liddick, P.F. Mantica, R. Broda, B.A. Brown, M.P. Carpenter, A.D. Davies, B. Fornal, M. Horoi, R.V.F. Janssens, A.C. Morton, W.F. Mueller, J. Pavan, H. Schatz, A. Stolz, S.L. Tabor, B.E. Tomlin, M. Wiedeking, Phys. Rev. C **72**, 054321 (2005).
- [37] M. Oinonen, U. Köster, J. Äystö, V. Fedoseyev, V. Mishin, J. Huikari, A. Jokinen, A. Nieminen, K. Peräjärvi, A. Knipper, G. Walter, and the ISOLDE Collaboration, Eur. Phys. J. A **10**, 123 (2001).
- [38] E. Caurier, Code ANTOINE, Strasbourg, 1989; E. Caurier and F. Nowacki, Acta Phys. Pol. **30**, 705 (1999).
- [39] M Honma, T. Otsuka, B.A. Brown, and T. Mizusaki, Eur. Phys. J. A **25**, 499 (2005).
- [40] S.N. Liddick, P.F. Mantica, B.A. Brown, M.P. Carpenter, A.D. Davies, M. Horoi, R.V.F. Janssens, A.C. Morton, W.F. Mueller, J. Pavan, H. Schatz, A. Stolz, S.L. Tabor, B.E. Tomlin, and M. Wiedeking, Phys. Rev. C **73**, 044322 (2006).